THE CAUCASUS TERRITORY HOT-COLD SPOTS DETERMINATION AND DESCRIPTION USING 2D SURFACE WAVES TOMOGRAPHY

Seyed Hossein Abrehdari[*,1,2], Jon K. Karapetyan[1],
Habib Rahimi[2], and Eduard Geodakyan[1]

[1]*Institute of Geophysics and Engineering Seismology, National Academy of Sciences, Gyumri, Armenia*
[2]*Institute of Geophysics, University of Tehran, Tehran, Iran*

Many questions have been raised about the thermal-mechanical development of plate tectonics boundary interactions, lithospheric processes, mantle activity, movement of faults, continental thinning, and generally the heat below the Earth's surface. The earthquake waves originate in the Earth's crust or upper mantle, and ricochet around the Earth's interior. They travel most rapidly through cold, dense regions, and more slowly through hotter rocks. In this paper, in order to identify and describe hot-cold spots in the Caucasus territory and better understand the regional tectonic activities based on the fast and slow wave velocity anomalies, the 2D tomographic maps of the Rayleigh wave dispersion curves were imaged. To obtain these maps in the ever-evolving collision zone of the Eurasian-Arabic plates, we performed a 2D-linear inversion procedure on the Rayleigh wave in a period ranging from 5 to 70 s (depth = ~200 km). To conduct this, ~1500 local-regional earthquakes ($M \geq 3.7$) recorded by the 48 broadband-short period stations from 1999 to 2018 were used. In this study, we assumed that the low-velocity tomography images or dark red-orange shades indicate hot spots (slow-regions), and high-velocity or dark blue-green-yellow shades imply cold spots (fast-regions). Therefore, by using the technique of increasing-decreasing the velocity anomaly in a wide area with complicated tectonic units the hot-zones and extensive cold-aseismic areas were described and investigated. Hence, for short-periods ($5 \leq T \leq 25$ s; $6.6 \leq$ depth ≤ 30.8 km) 15 hot spots were determined. The result for medium-periods ($30 \leq T \leq 45$ s) shows two hot spots with a depth of ~108 km. For long-periods (depth ~200 km), most part of the study area is covered by ultra-low-velocity anomalies as permanent hot spots.

Keywords: Caucasus territory, hot-cold spots determination, 2D surface wave tomography, Geothermal resources, 2D linear inversion

1 INTRODUCTION

To map the Earth's interior the seismic waves chart movement (traces) generated by earthquakes that have been recorded by a worldwide network of seismometers are used. Each recorded wave trace reveals much useful information from the extent and density of the Earth's deepest regions.

According to the seismic tomography images of [*Perkins*, 2019] studies of the Earth, the colors show anomalies in rigidity, which correlate with temperature anomalies (https://www.iris.edu/hq/inclass/fact-sheet/seismic_tomography). The dark blue-green-yellow shades mean colder and stiffer rocks (Cold spots) that are the remnants of an old tectonic plate that has been subducted underneath the Earth plates (large cold and aseismic area during million years) and dark red-orange shades mean warmer and weaker regions (hot spots).

It is believed that a hot spot is a location on the Earth's surface that has experienced active volcanism for a long period and is fed by an underlying mantle that is anomalously hot compared with

---
*Corresponding author: abrehdari@ut.ac.ir (S. H. Abrehdari)

the surrounding mantle. The origins of the concept of hot spots lies in the work of [*Wilson*, 1963], who postulated that the formation of the hot spot is conditioned by the slow movement of a tectonic plate across a hot region beneath the surface.

As the result of chemical interactions in volcanic zones, tectonic activities, high temperatures, and pressures in the Earth's interior some of the rocks are melted, the solid behavior becomes plastic and geothermal zones (hot spots) arise. Some 40–50 such hot spots around the globe have been identified (Figure 1).

Estimates for the number of hotspots supposed to be fed by mantle plumes have ranged from about 20 to several thousand, over the years, with most researchers considering a few tens to exist. Hawaii, Réunion, Yellowstone, Galápagos, and Iceland are some of the most active volcanic regions to which the hypothesis is applied [*Foulger*, 2010; *Wright*, 2000]. However, it is important to bear in mind that these are simply theories and that no definitive solution has been arrived at.

Hot spots (close to the Earth's surface) are the same geothermal resources and are useful for identifying sources of geothermal energy. For example, some countries such as Iceland (Nesjavellir Geothermal Power Plant), New Zealand (Wairakei Geothermal Power Plant), Turkey (Efeler geothermal power plant), and NW Iran (use water from hot or hydrothermal springs) are using this energy.

This paper attempts to generate the 2D tomographic inversion of Rayleigh wave velocity dispersion maps to identify and describe hot-cold spots inside the Earth based on *fast* and *slow* wave velocity anomalies. To do this, the Rayleigh wave group velocity dispersion curves for each source-station path (single-station method) are estimated using Hermann's do_mft package [*Herrmann*, 2013].

Then, using a 2D-linear inversion method developed by [*Ditmar and Yanovskaya*, 1987] and [*Yanovskaya and Ditmar*, 1990], the 2D group velocity maps were generated. Some studies of the crustal structure have been conducted related to the estimation of the crustal thickness beneath this region (e.g., NW Iran: [*Gheitanchi*, 1996]; Caucasus: [*Martin et al.*, 2007]; Eastern Anatolian Accretionary Complex (EAAC): [*Skobeltsyn et al.*, 2014]). These maps show excellent agreement with the results of the previous studies and many of the geological features of the Caucasus territory.

The main purpose of this study is to investigate the hot-cold spots in the Caucasus based on scattering characteristics of the wave velocity increasing and decreasing using 2D tomographic maps. In the Caucasus dominion, no study has been conducted entitled hot-cold spots using surface wave tomography on a large-small scale yet. This study benefits from a rich earthquake database (1999–

2018) and new permanent seismic stations installed in NW Iran, Russia, Armenia, Turkey, Azerbaijan, and Georgia, which provides much better ray path coverage in the Caucasus for the resolution of tomographic images. Also, to provide more useful information to researchers about the hot-cold zones, the results of the performed previous tomographic studies in the Caucasus were used.

2   CAUCASUS GENERAL INFORMATION

The Caucasus region is a well-known and complex area in aspects of various ongoing tectonic evolution processes. The structure of the Caucasus mountain region and surrounding areas is primarily controlled by the collision and continuing convergence of the Arabian-Eurasian plates. Over time, this motion led to subsequent collision stages between Arabia and smaller continental blocks resulting from the break-up of Gondwana until the final closure of the Neo-Tethys Ocean.

Because of this geodynamic evolution, a complex geological structure characterized by important lateral variations in age, composition, and tectonic style has formed [*Hatzfeld and Molnar*, 2010]. Greater Caucasus (GC), Lesser Caucasus (LC), East Anatolian Accretionary Complex (EAAC), Bitlis Massif (BM), Pontide (PN), NW Iran, Tlesh (TAL), South Caspian Basin (SCB), Kura Basin (KB), Rioni Basin (RB) and Eastern Blake Sea Basin (EBSB) are some parts of the Arabia-Eurasia collision.

The Greater Caucasus mountains are an orogenic belt that was raised as a result of the collision, with altitudes of more than 5 km above sea level and 1300 km in the NW-SE direction between the Black Sea and the southern basin of the Caspian Sea. The convergence between Arabia and Eurasia began in Late Cretaceous [*Golonka*, 2004].

According to some studies (e.g., [*Copley and Jackson*, 2006; *Jackson*, 1992]), these continent-continent collisional tectonic processes has begun at about 12 Ma. The Caucasus region is compressed between Arabian-Eurasian plates and due to N-S compression expanded the main seismo-active structures in NW Iran, GC, LC, and EAAC. The fault zones include reverse strike-slip, strike-slip sinistral, strike-slip dextral, wrench, and major thrust faults with WNW-ESE direction are developed (Figure 7). Further, there are several large Neogene-Quaternary strato-volcanoes (< 0.4 Ma – 6.5 Ma) [*Bavali et al.*, 2016] such as Elbrus that is located in this region.

According to some studies [*Ismail-Zadeh et al.*, 2020; *Karapetyan et al.*, 2020], the Caucasus ranges include the Greater Caucasus, that is consisting mostly of Paleozoic metasedimentary rocks and granitoids, Jurassic sediments, Mesozoic and Cenozoic volcanism, and the Lesser Caucasus that
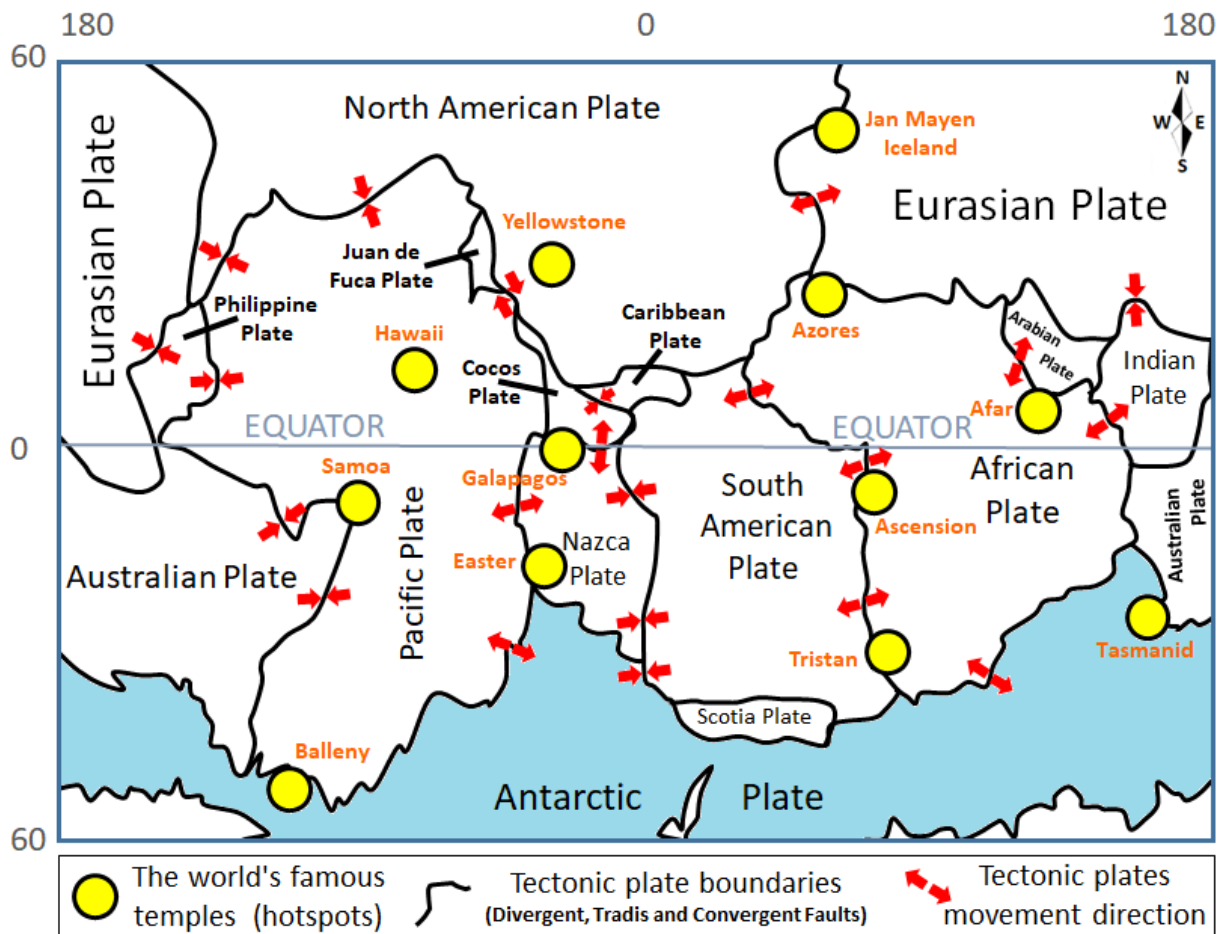
Figure 1: Mantle plume locations (yellow circles) are the world's most famous (hot spots). Figure retrieved from: https://www.sciencelearn.org.nz/images/350-tectonic-plate-boundaries, University of Waikato.

consists of Paleozoic granitoid metamorphic basement overlain unconformably by shelf carbonates of Paleozoic Triassic age, respectively. In this complex area, there are complicated geological structures and large volcanic complexes and basins.

3   DATA AND STUDY AREA

The study area is the territory of the Caucasus (Longitude: 38°–53°; Latitude: 37°–44°). The dataset used for tomography consists of ~1500 local-regional events with magnitude $M \geq 3.7$, which have been collected by 48 broadband and short-period Seismic Network of Incorporated Research Institutions for Seismology (IRIS) including Armenia (GNI), Georgia (GO), Turkey (TK, TU), Azerbaijan (AB), as well as earthquake data recorded by the Iranian Seismological Center (IRSC), International Institute of Earthquake Engineering and Seismology (IIEES), and the temporary network of the Institute for Advanced Studies in Basic Sciences (IASBS) from 1999 to 2018 (Table 1). The study area, distributions of earthquakes, and seismic stations used in the analysis are shown in Figure 2 and Figure 7. The Geological units, faults, volcanoes, rivers, and basins that were used for the interpretation of the 2D tomography maps in the study area are shown in Figure 7.

3.1   Ray paths distribution and resolution parameters

The resolution of group velocity maps depends more on the density of the paths and their balance distribution (crossing paths). In tomographic studies related to seismic events data, these two parameters depend on the distribution of the earthquakes and the geometry of the seismic array which can limit the number of available paths for some directions which are almost beyond our control.

According to [Yanovskaya, 1997] and [Yanovskaya et al., 1998], the stretching of the averaging area and the mean size parameters are used to estimate the lateral resolution. For 2D tomography problems, a function $S(x, y)$ for different orientations
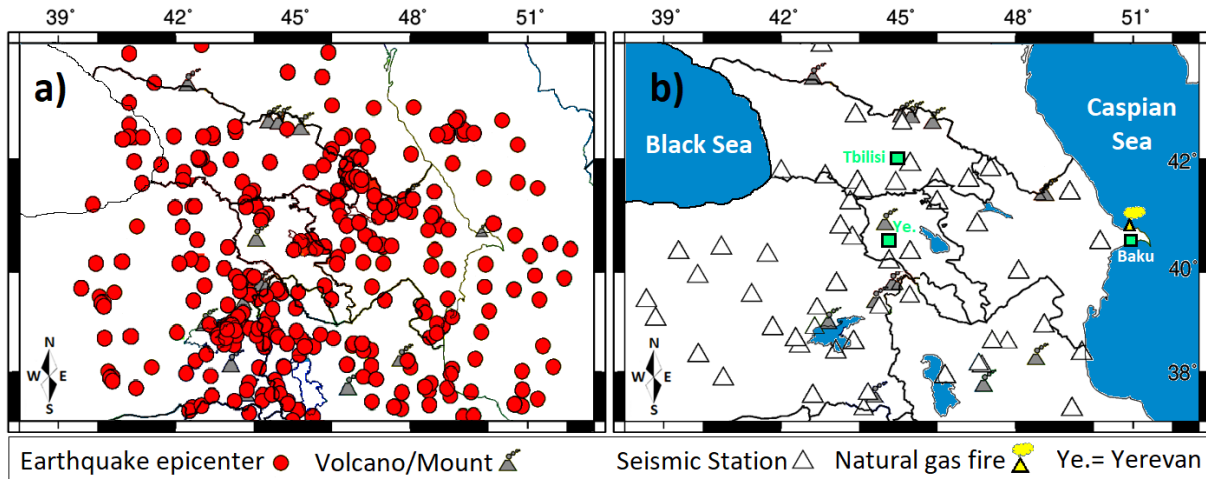
Figure 2: a) The seismic events (red circles) and b) locations of the stations used in this study.

of the coordinate system is used to determine the sizes of the averaging area along different directions. The averaging area which gives us an idea of the obtained resolution can be approximated by an ellipse centered at a point, with axes equal to the largest $S_{max}(x,y)$ and the smallest $S_{min}(x,y)$ values of $S(x,y)$. The smallest $S_{min}(x,y)$ and largest $S_{max}(x,y)$ axes of the ellipse are calculated, and the resolution in each point is given the mean size of the averaging area:

$$L = (S_{min}(x,y) + S_{max}(x,y))/2. \quad (1)$$

As the resolution is closely correlated to the density of the crossing ray paths in each cell, it is clear that small values of the mean size of the averaging area L (corresponding to high resolution) should appear in the areas that are crossed by a large number of ray paths and vice versa.

The second parameter is the stretching (ex or ε) of the averaging area, which provides information on the azimuthal distribution of the ray paths and is given by the ratio:

$$\text{ex or } \varepsilon = (S_{max}(x,y) - S_{min}(x,y))$$
$$/(S_{max}(x,y) + S_{min}(x,y)), \quad (2)$$

where S_{max} and S_{min} are the large and small elliptical focal lengths. According to the study [*Yanovskaya*, 1997], large values of the stretching parameter (usually > 1) imply that the paths that have a preferred orientation and along this preferential direction are likely to be quite small. On the contrary, small values of the stretching parameter imply that the paths are more or less uniformly distributed along all directions; hence the resolution at each point can be represented by the mean size of the averaging area. By calculating the $\overline{S}_{max}$, $\overline{S}_{min}$ parameters and L in this study, the value of $\varepsilon = 0.6985 \sim 0.7$ was obtained.

Figure 3a–c shows the number of paths in each period, distribution of stations-earthquakes ($T = 10$ s, $\alpha = 0.2$), and ray coverage between seismic events epicenters-stations in the study area, respectively. Distribution of stations and earthquakes controls the amount of stretching parameters and data density. The mean size of the averaging area of our tomographic results is of the order of 183.57 (Table 2) in most part of the study region. The values of the stretching of the averaging area are between 0.5 and 0.95 in most part of the study area at the fourteen periods. This indicates that the azimuthal distribution of the paths is sufficiently uniform and the resolution is almost the same in any direction. The averaging area value is larger than ~150, with its maximum equal to ~2400. The dense rays path distribution (Figure 4 and Figure 6, $\alpha = 0.2$) controls the reliability and the high resolution of tomography results (red shads in Figure 4 – averaging area (L). For more details, in this case, see subsection 4.2.

Therefore, stretching (ε) and averaging area (L) values are two parameters that indicate the orientation and resolution of the different areas within the study area for each period and at any latitude (Y) and longitude (X) direction. Figure 4 illustrates the variation of these two parameters for some periods. Figure 4 a–f shows the cell size of $0.2° \times 0.5°$ (20×50 km^2) for the stretching, data density, and averaging area parameters at a period 5–70 s (generated by MATLAB software). [*Yanovskaya*, 1997] methodology is used to calculate the spatial resolution, which varies from 20 to 50 km in our study region. We constructed the 2D tomography velocity model in the Caucasus by inverting the pure path Rayleigh wave dispersion curves at ($35 \times 30 = 1050$) nodes using a grid with a cell size of $0.2° \times 0.5°$ (20×50 km^2).

In this study, the various α values (0.1, 0.2 and 0.3) were tested and the number of ray paths pass-
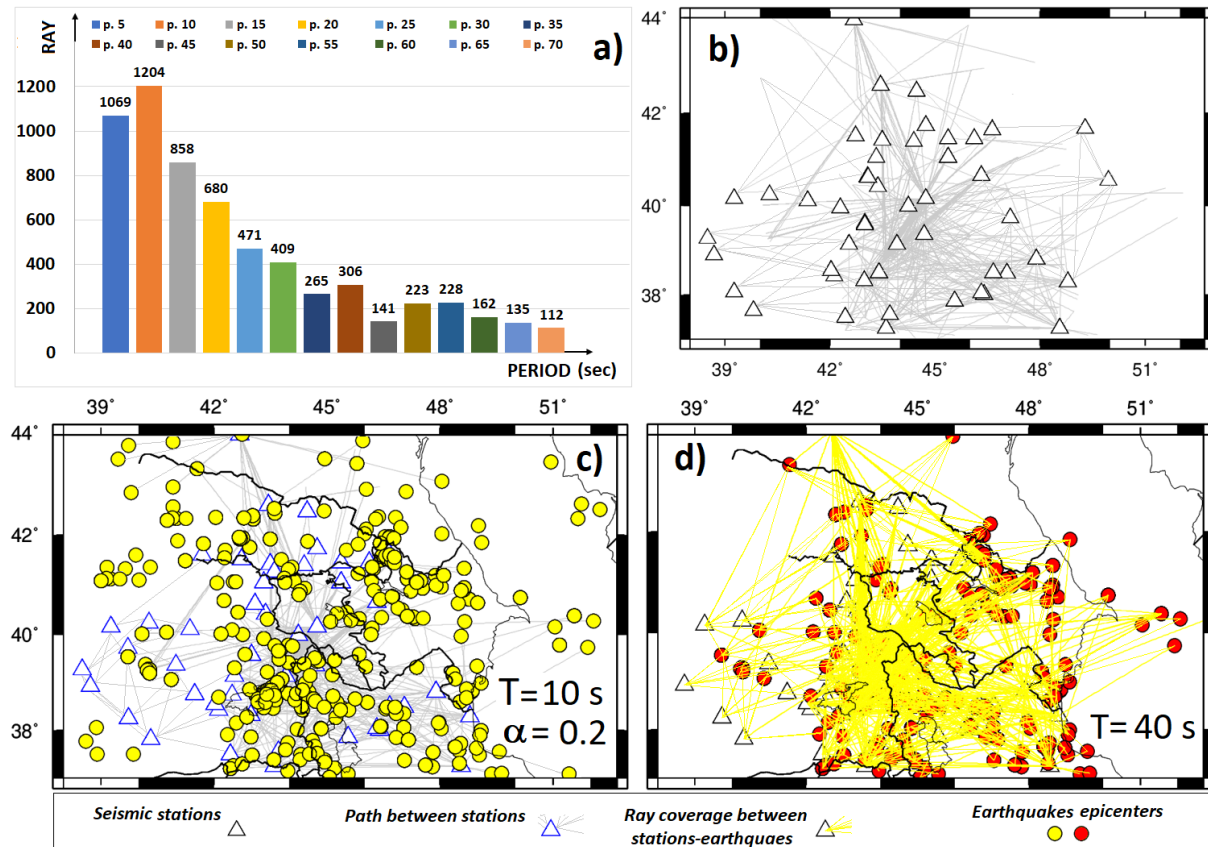
Figure 3: a) The number of ray paths used in the tomography inversion respective to the period in this study. b) The distribution of seismic stations and interstation path coverage. c) The appropriate value of $\alpha(0.2)$ selected for performing tomography at a period of 10 s. d) shows the sample of events-stations rays coverage (yellow lines) at a period of 40 s.

ing through each cell was observed and selected. So, the checkerboard test was ignored and it is not required to perform. This method is much more useful than the checkerboard test (Figure 6).

Also, in order to have a good quality data bank in the time domain, we used SNR = 3 for the initial processing of data in different periods. Then, by choosing the proper regularization parameter (α) in the computer code, we improved the resolution of the tomography images by observing the most data and the beam passing through each cell.

4 Methodology

4.1 Dispersion estimation

After preparing the earthquakes waveform and preliminary corrections on it, for each station-earthquake pair (single-station method), the group velocity dispersion curve of Rayleigh waves by applying Herrmann's do_mft package [*Herrmann*, 2013] to the vertical component (Z) of motion on each event is estimated. Modified sacmft96 work about problems with the improper station and component specifications in Sac-files. Sacmft96

is called do_mft for interactive analysis of group velocities and spectral amplitudes. SAC (Seismic Analysis Code) is a general-purpose interactive program designed for the study of sequential signals, especially time series data.

In fact, the frequency-time analysis of surface waves is used to estimate the dispersion curves. This method is used for estimating the phase and group velocity of surface waves. It passed the pre-processed signal through a system of narrow-band filters in which the central frequency is varying and the amplitude of filter outputs is visualized in time and frequency domains. Then, on the do_mft diagram, the group velocity dispersion curve for each path is obtained. Figure 5 shows an example of determining the group velocity dispersion curve for the vertical component (Z) of the Oni (ONI) station using do_mft processing.

To conduct this, we applied Herrmann's do_mft package on waveforms of ~1500 earthquakes recorded by the 48 stations in the Caucasus region. We then processed more than ~34,000 vertical components (Z) of dispersion curves (Figure 5e). For this purpose, first, in the Ubuntu system, the earthquake data (miniSEED format) was

Table 1 : Station and network codes, coordinates, and data center website considered in this study.

Station Code	Station name	Longitude (°)	Latitude (°)	Network Code	Data Center Website
GNI / GSS	Garni, Armenia	44.7241	40.1341	IU (IRIS/USGS)	A0: National Seismic Network of Armenia https://www.fdsn.org/networks/?initial=G
GANJ	Ganja, Azerbaijan	46.3297	40.6519	IU (IRIS/USGS)	AB: National Seismic Network of Azerbaijan https://www.fdsn.org/networks/detail/AB/
QZX	Qazah, Azerbaijan	45.3721	41.0481	IU (IRIS/USGS)	
ZKT	Zakatala, Azerbaijan	46.6311	41.6411	IU (IRIS/USGS)	
AKH	Akhalkalaki	43.4929	41.4111	IU (IRIS/USGS)	GO: National Seismic Network of Georgia https://www.fdsn.org/networks/detail/GO/
BATM	Batumi	41.6936	41.6041	IU (IRIS/USGS)	
BGD	Ninotsminda	43.5985	41.2645	IU (IRIS/USGS)	
CHVG	CHKVALERI	42.0841	42.71833	IU (IRIS/USGS)	
DDFL	Dedoflistskaro	46.1183	41.44580	IU (IRIS/USGS)	
DGRG	DGRG - GAREJI	45.3731	41.45072	IU (IRIS/USGS)	
GUDG	Gudauri	44.4772	42.4646	IU (IRIS/USGS)	
KZRT	Kazreti	44.3987	41.3866	IU (IRIS/USGS)	
LGD	Lagodekhi	46.2421	41.8343	IU (IRIS/USGS)	
ONI	Oni	43.4524	42.5905	IU (IRIS/USGS)	
SEAG	TbilisiSea	44.8036	41.7635	IU (IRIS/USGS)	
TBLG	Delisi, Georgia	44.7381	41.7309	IU (IRIS/USGS)	
TRLG	Trialeti	44.1017	41.5392	IU (IRIS/USGS)	
ANDN	ANDIRIN, TURKEY	37.5811	36.3452	IU (IRIS/USGS)	TU: National Seismic Network of Turkey (DDA) https://www.fdsn.org/networks/detail/TU/
AYDN	TASOLUK, TURKEY	37.6608	27.8792	IU (IRIS/USGS)	
BALY	BALYA, TURKEY	39.7403	27.6195	IU (IRIS/USGS)	
BORA	ESKISEHIR, TURKEY	39.8801	30.4534	IU (IRIS/USGS)	
DIGO	KARS, TURKEY	40.4147	43.3742	IU (IRIS/USGS)	
EPOS	POSOF, TURKEY	41.5035	42.7279	IU (IRIS/USGS)	
ERBA	ERBA, TURKEY	40.6814	36.7547	IU (IRIS/USGS)	
HAKT	HAKKARI, TURKEY	37.5579	43.7071	IU (IRIS/USGS)	
ILGA	ILGAZ, TURKEY	41.0521	33.7165	IU (IRIS/USGS)	

Table 1 : Station and network codes, coordinates, and data center website considered in this study (continued).

Station Code	Station name	Longitude (°)	Latitude (°)	Network Code	Data Center Website
KELT	KELKIT, TURKEY	40.1486	39.2556	IU (IRIS/USGS)	
KEMA	KEMALIYE, TURKEY	39.2688	38.4932	IU (IRIS/USGS)	
VANB	Gevas, Van sir	39.57798	28.63232	IU (IRIS/USGS)	TK: National Strong-Motion Network of Turkey (TR-NSMN) https://www.fdsn.org/networks/detail/TK/
CUKT	Gerede, Bolu	40.7924	32.2059	IU (IRIS/USGS)	
TASB	Tefenni, Burdur	37.3160	29.7791	IU (IRIS/USGS)	
MLAZ	Merkez, Edirne	41.6704	26.5858	IU (IRIS/USGS)	
AKDM	Merkez, Erzurum	39.8733	41.2226	IU (IRIS/USGS)	
AGRB	Iskenderun, Hatay	36.5571	36.1747	IU (IRIS/USGS)	
SIRT	Karaburun, Izmir	38.6390	26.5127	IU (IRIS/USGS)	
GURO	Marmaris, Mugla	36.8394	28.2448	IU (IRIS/USGS)	
KARS	Susehri, Sivas	40.1692	38.1063	IU (IRIS/USGS)	
DIGO	Dursunbey, Balike	38.2963	43.1197	IU (IRIS/USGS)	
FTBB	—	46.3944	38.0171	IRSC	Iranian Seismological Center (IRSC) http://www.irsc.ut.ac.ir/istn.php
TBZ	Tabriz	46.1498	38.2348	IRSC	
TVRZ	—	46.6675	38.5042	IRSC	
BRND	—	48.5680	37.2483	IASBS	Institute for Advanced Studies in Basic Sciences (IASBS), https://iasbs.ac.ir
SARA	Sarab	45.56.54	37.8634	IASBS	
GRMI	Germi (Ardebil)	47.8940	38.8100	INSN	Iranian National Seismological Center http://www.iiees.ac.ir/
MAKU	Maku (Urmia)	44.6829	393550	INSN	http://www.iiees.ac.ir/en/iranian-national-broadband-seismic-network/
KIV	Kislovodsk, Russia	43.9562	42.6888	IRISDMC	II: Global Seismograph Network — IRIS/IDA https://www.fdsn.org/networks/detail/II/

converted to a SAC file format and then the fundamental mode of the Rayleigh wave for each vertical component (Z) using the do_mft package was determined.

Figure 5a shows the raw, radial component, and the processed waveform. Figure 5b shows the dispersion curve measurement by do_mft to separate the fundamental mode of earthquake data waveform. Figure 5c shows the picked dispersion curve related to the energetic part of the signal (red area)

in b for the earthquake recorded in the Oni seismic station (ONI, Georgia).

In the single-station method, since estimating the dispersion curves depends on the basic parameters of earthquakes such as magnitude, epicentral distance, depth, etc.; different period ranges by applying do_mft to every epicenter-station pair are attained; hence, for different periods we have various path numbers. Finally, a set of dispersion curves for the fundamental mode Rayleigh wave in
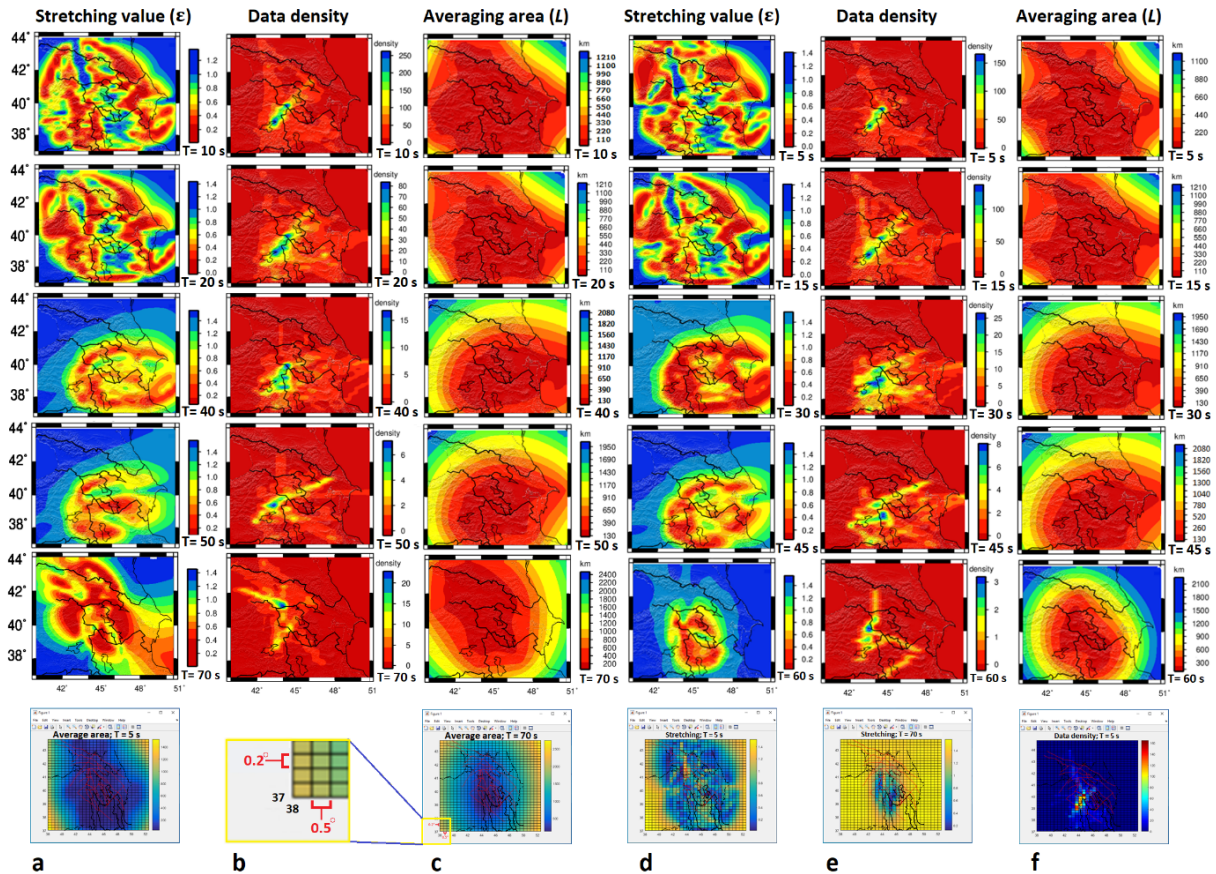
Figure 4: Resolution of parameters map: stretching value (ε), data density, and average value (L) for short-periods of 5, 10, 15 and 20 s; medium-period of 30, 40 and 45 s; and long-periods of 50, 65, and 70 s in this study. Figures a, c–f show the size of the cells $0.2° \times 0.5°$ (20×50 km^2) for parameters of stretching, averaging area, and data density for the shortest and the longest periods (generated by MATLAB software). Fig. b shows the zoomed cells.

the period range from 5 to 70 s to create 2D tomography maps was estimated (Figure 5e). The periods greater than 70 s in this study (see Figure 5e), due to poor coverage of dispersion curves, which leads to poor coverage of the rays to conduct the tomography images were ignored.

4.2 Two-dimensional surface wave tomography

When earthquake occurs, seismic waves burst outwards and travel most rapidly through cold, dense regions and more slowly through hotter rocks. Waves travel faster through cold-rigid material (like a subduction plate inside the mantle) and pass through warmer materials more slowly (like hot rocks rising to the surface). Seismic tomography is like taking a Computed Tomography or CAT scan of the Earth. In a method similar to CT scans, scientists instead use seismic waves to make images of the Earth's interior.

Concerning the interpretation of tomography images [Perkins, 2019] of the Earth, the colors show anomalies in rigidity, which correlate with temperature anomalies. Hence, the dark blue-green-yellow shades mean colder and stiffer rock (cold spots areas) and dark *red-orange* shades mean warmer and weaker regions (hot spots areas). *Thus, in this study, the tomography images with dark red-orange shades show low-velocity (slow-hot) zones and dark blue-green-yellow shades indicate high-velocity (fast-cold) areas.*

In order to construct group velocity distribution maps in periods ranging from 5 to 70 s, a 2D-linear tomographic inversion technique developed by [*Ditmar and Yanovskaya*, 1987] and [*Yanovskaya and Ditmar*, 1990] was used. This methodology is a generalization of the classical 1-D method of [*Backus and Gilbert*, 1968].

The study region was parametrized into grids with a cell size of $0.2° \times 0.5°$ and with proper regularization parameters to provide relatively smooth maps with small data misfits. The same regularization parameters were used for producing the maps, before and after the impoundment. The resolution of the data set is controlled by the average path length, density of paths, and azimuthal coverage.

Table 2 : Fluctuations in the parameters of resolution: stretching value (ε), averaging area (L) value (km), and data density. Also, the table shows the velocity (km/s), depth (km), and possible Moho-LAB-LVZ depth (km) discontinuities in each period of 5 to 70 s.

Period (Sec.)	Possible location of Moho-LAB-LVZ (km)	Stretching value (ε)	Averaging area (L) value (km)	Data density value	Velocity (km/s)	Depth (km)
5	—	$0.2 < \varepsilon < 1.4$	150	110	$2.0 \leq V \leq 4.0$	$6.6 \leq Dep. \leq 13.33$
10	—	$0.2 < \varepsilon < 1.2$	250	110	$2.0 \leq V \leq 4.2$	$13.33 \leq Dep. \leq 28$
15	Moho (22-30)	$0.2 < \varepsilon < 1.4$	190	110	$2.2 \leq V \leq 3.0$	$22 \leq Dep. \leq 30$
20	Moho (40-57)	$0.2 < \varepsilon < 1.4$	80	110	$2.5 \leq V \leq 4.4$	$33.33 \leq Dep. \leq 57.33$
25	—	$0.2 < \varepsilon < 1.4$	40	110	$2.3 \leq V \leq 3.2$	$38.33 \leq Dep. \leq 53.33$
30	—	$0.3 < \varepsilon < 1.4$	29	160	$2.3 \leq V \leq 3.4$	$46 \leq Dep. \leq 68$
35	—	$0.4 < \varepsilon < 1.4$	25	195	$2.7 \leq V \leq 3.6$	$63 \leq Dep. \leq 84$
40	—	$0.1 < \varepsilon < 1.4$	15	115	$1.7 \leq V \leq 3.7$	$45.33 \leq Dep. \leq 98.66$
45	—	$0.1 < \varepsilon < 1.4$	8	250	$3.2 \leq V \leq 3.6$	$96 \leq Dep. \leq 108$
50	LAB (96-175)	$0.2 < \varepsilon < 1.4$	7	250	$1.75 \leq V \leq 5.0$	$58.33 \leq Dep. \leq 166.66$
55	—	$0.1 < \varepsilon < 1.4$	10	195	$1.5 \leq V \leq 4.75$	$55 \leq Dep. \leq 174.16$
60	LVZ (104 ≥ 174)	$0.1 < \varepsilon < 1.4$	3	220	$1.6 \leq V \leq 2.7$	$64 \leq Dep. \leq 108$
65	—	$0.1 < \varepsilon < 1.4$	3	290	$1.5 \leq V \leq 3.5$	$65 \leq Dep. \leq 151.66$
70	—	$0.2 < \varepsilon < 1.4$	2	300	$1.4 \leq V \leq 3.4$	$65.33 \leq Dep. \leq 158.66$

In addition to group velocity maps, the corresponding resolution information will be provided at each period. The methodology [*Yanovskaya, 1997*] is used to calculate the spatial resolution at each point and in different directions. *Therefore, it is clear that checkerboard testing is not required and the averaging area maps (red shades) show the highest resolution in each period by choosing the proper regularization parameter(α).* The main advantage of this method is that in the cases of uneven distribution of surface wave paths, it works well. The dataset in this method is the travel times along different paths at each period that were calculated by Herrmann's do_mft package. The method estimates the lateral variation of group velocity V_x at each period.

The lateral group velocity distribution could be estimated by minimizing the following function:

$$(d - Gm)^T (d - GM) + \alpha \iint |\nabla_m(X)|^2 \, dX = \min , \quad (3)$$

where

$$m(X) = (V^{-1}(X) - \left(V_0^{-1}\right) V_0, \quad (4)$$

where

$$d_i = T_i - T_{i0}, \quad (5)$$

$$(Gm)_i = \iint G_i(X)m(X)dX = \int_{L_{oi}} m(X)\frac{ds}{V_0} , \quad (6)$$

$$\iint G_i(X)dX = \int_{L_{oi}} \frac{ds}{V_0} = t_{i0}. \quad (7)$$

In the relations (3–7), $X = (\theta, \varpi)$ is the position vector, V_0 is the velocity corresponding to a starting model, t_i is the observed travel time along the i_{th} path, t_{io} is the travel time calculated for the starting model, α is a regularization parameter, t_{io} is the length of the i_{th} path and s is the segment along which the inversion is performed.

The regularization parameter (α) that depends on the accuracy of the data, is the trade-off between the fit to the data and the smoothness of the resulting velocity distribution. A decrease in α gives a sharper solution region with an increase in solution error, whereas an increase in α leads to a smoothing of the solution region with a decrease in solution error [*Yanovskaya et al., 1998*].

The parameter α controls the trade-off between the fit to the data and the smoothness of the resulting group velocity maps. Therefore, to improve the resolution and for having a real model, we tested various values of the regularization parameter (α).
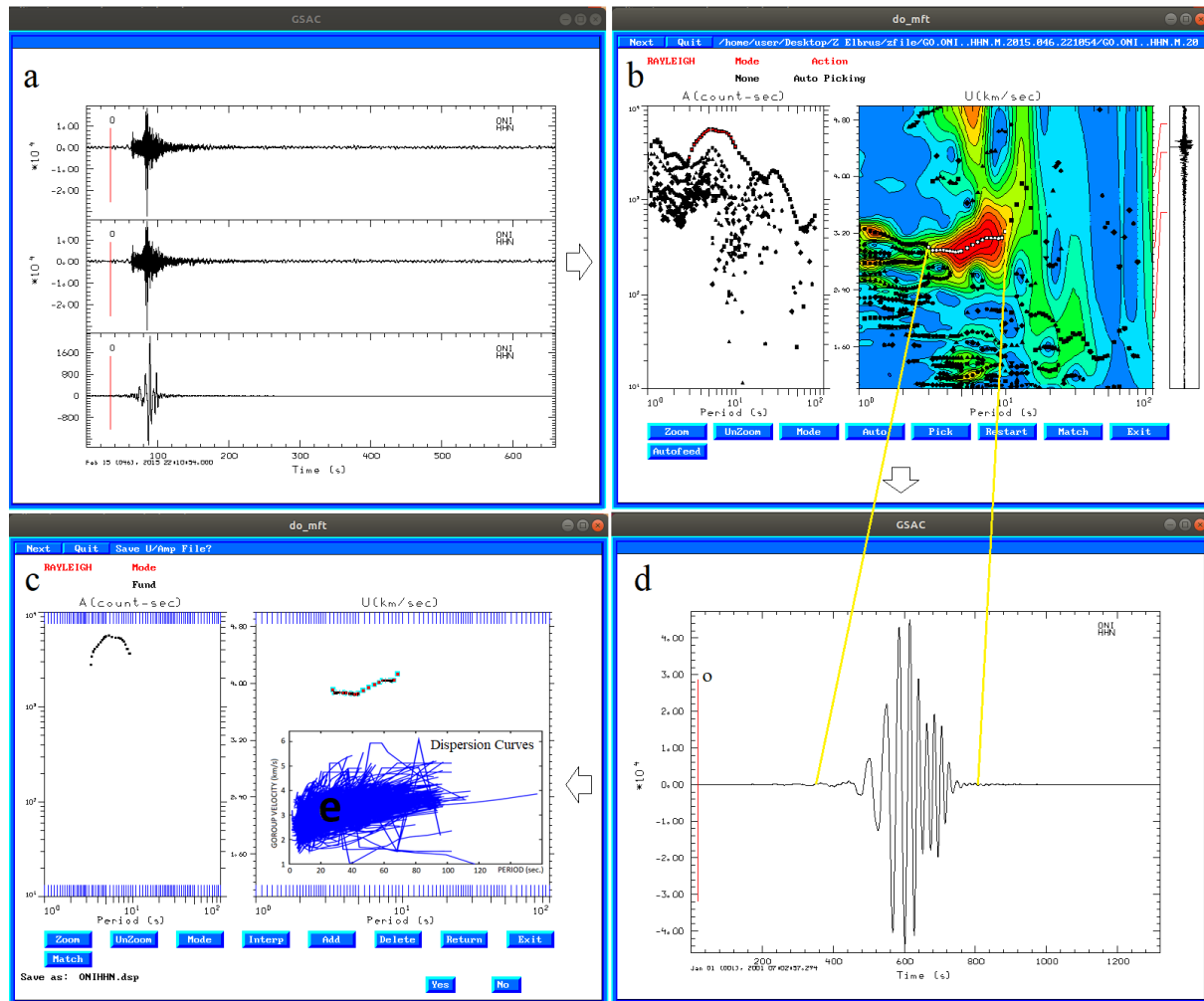
Figure 5: a) Raw, radial component and cleaned seismogram waveform (up to down). b) An example of determining group velocity dispersion curve using Herrmann's do_mft package for the vertical component (*Z*) of the Oni (ONI- Georgia) seismic station. Earthquake source parameters and the recording station name are mentioned on the dispersion curve plot. The raw waveform is given in the right-hand rectangular block. c) The picked dispersion curve related to the energetic part of the signal (red area) in b. The vertical red lines (with the alphabet 'O' above them) show the onset of chosen pickfile by SAC software (automatic default of start reading of arrival time). e) Dispersion curves (~34000 curves).

We chose $\alpha = 0.2$ which gives relatively smooth maps with small solution errors which were conducted by testing different α values and observing the number of rays passing through each cell size of $0.2° \times 0.5°$ by running the specialized computer codes in MATLAB software which is used in this study (Figure 6). Also, see subsection 3.1.

As shown in Figure 6, choosing the proper regularization parameter ($\alpha = 0.2$), reflects the uniformly distributed ray paths for conducting the tomography (for averaging area and stretching red shades). Finally, by selecting the compatible regularization parameter and using the GSAC, GMT software, and computer specialized codes in the Ubuntu operating system and MATLAB software, the 2D tomography group velocity, stretching, data density, and averaging area maps were plotted and estimated in period ranges from 5 to 70 s (Figure 4).

In the papers [*Yanovskaya*, 1997] and [*Yanovskaya et al.*, 1998] it was proposed to use two parameters to estimate the lateral resolution: the mean size and the stretching of the averaging area. The resolution is directly controlled by the coverage of the ray paths and the distribution of stations and earthquakes. Therefore, determining the compatible regularization parameters (ℵ) plays a very important role in the resolution of tomography images (Figure 4 and Figure 6).

Moreover, by determining the compatible regularization parameter (α) and thus correctly estimating the mean size and the stretching of the av-
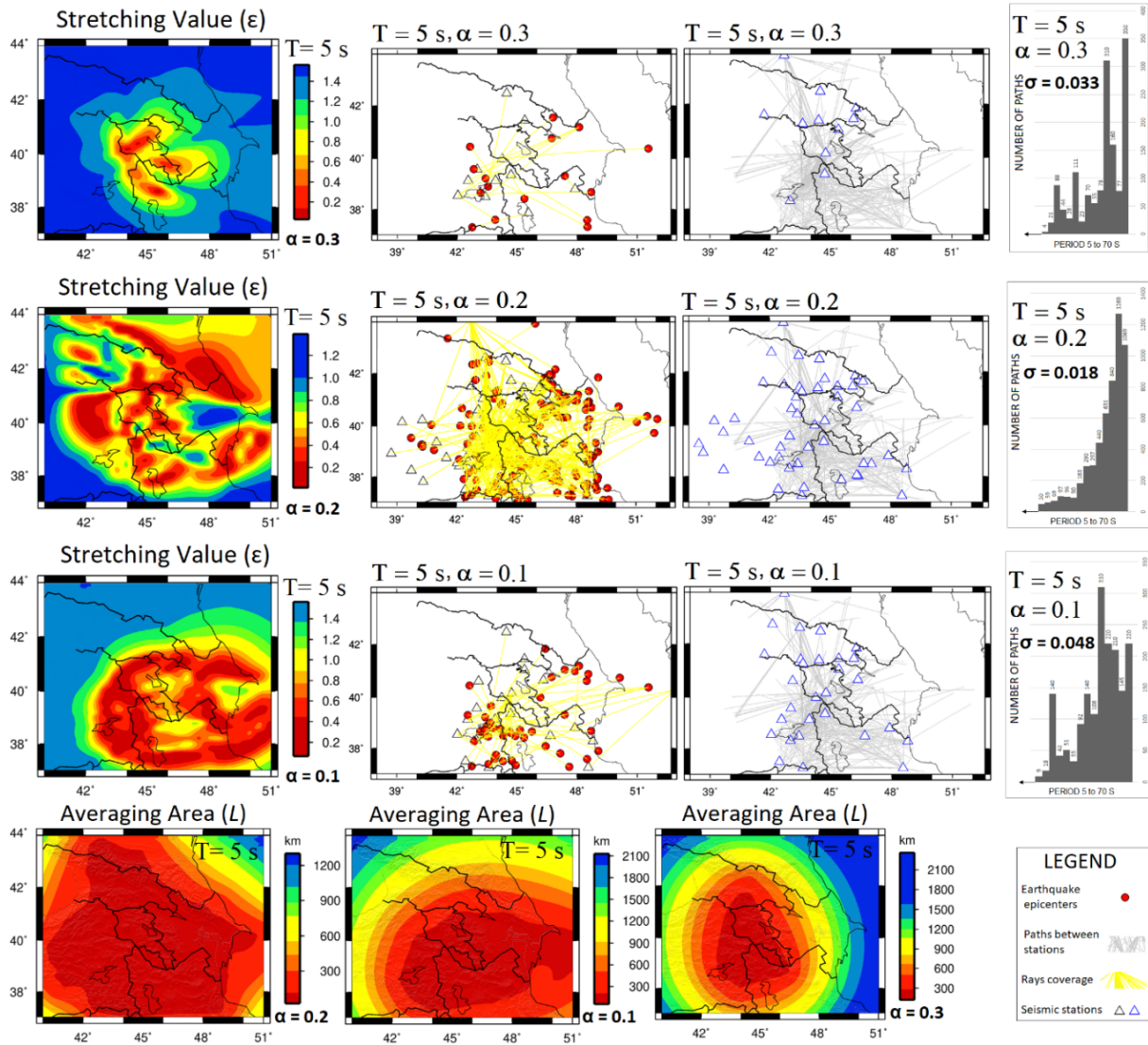
Figure 6: Calculations of group velocity maps are imaged for several regularization parameters (α). A decrease in α gives a sharper solution region with an increase in solution error, whereas increasing α results in smoothing of the solution region with decreasing solution error. The small solution errors by testing different α values ($\alpha = 0.1$, 0.2, and 0.3) and observing the number of rays path passing through each cell size of $0.2° \times 0.5°$ by running the specialized computer codes in MATLAB software, which was determined in this study.

eraging area, there is no need for a checkerboard test for resolution, and gives relatively smooth maps with small solution errors.

Another criterion that controls the quality of the solution is the comparison between the initial mean square travel time residual and the remaining (unaccounted) residual σ. It is assumed that the unaccounted residuals are random, so σ_m can be accepted as an estimate of the standard deviation (error) of the data, which allows a standard error of the solution σ_m to be computed. Therefore, in this study, the value of σ_m is used for the selection of the appropriate data: if the travel time residual for one path is larger than 3σ, this path is eliminated from the dataset and the solution is re-

calculated [*Yanovskaya et al.*, 1998]. The standard deviation (σ) with selecting the regularization parameter $\alpha = 0.2$ is reasonably low which shows the stability of the method. (Figure 6).

5   Hot-cold spots determination and description using 2D tomography velocity maps

As mentioned earlier, the wave travels more rapidly through cold, dense regions, and more slowly through hotter rocks and zones. *Thus, in this study, we assumed that each low-velocity (slow) region with a dark red-orange shade is a hot spot and each high-velocity (fast) region with a dark blue-*

green-yellow shade is a cold spot. Hence, to identify and describe hot-cold spots inside the Earth of the study area based on the increase and decrease of the wave velocity anomalies, the 2D tomographic velocity maps obtained in Figure 8 were generated.

A schematic diagram of Figure A.1 has been depicted to better understand the hot-cold spots procedure inside the Earth. Figure A.1 shows the physical processes within the Earth's upper mantle that lead to the generation of magma in steps A to D for different plate tectonic settings. Tomographic maps with distinct velocities over short periods of 5 to 25 s (equivalent to a depth of 6 to 53 km), are more sensitive to the structure of the upper to lower crust and Moho. These short periods represent sediments in the basins, chemical interactions of hydrocarbon resources, molten material, and magma chambers beneath volcanoes and Moho discontinuity. These areas can be considered temporary and unstable hot and cold spots.

These periods, which are also known as the crust, include soil, vegetation growth, construction, surface-groundwater, oil-gas resources, magma chambers, metallic, non-metallic mines, and chemical interactions. Although, some researchers believe that slow velocities in the crust or upper mantle under regions of active volcanism do not require "hot spot" (i.e., plume-related) magmatism. These could simply reflect decompression melting and/or crustal melting following slab-rollback, delamination, or breakoff.

The lithosphere-aesthenosphere and upper mantle are the sources of volcanic lava and the origin of some earthquakes in the mantle and remnants of the old tectonic plate. So, short periods (T = 5–25 s) can be considered *temporary and unstable hot and cold spots*.

Dark red spots that are seen below the chain of volcanoes (e.g., Elbrus, Ararat, Aragats, Kazbek), upon some segments of faults (e.g., PSSF, NTF) and basins (e.g., SCB, KB, EBSB, RB) in the study area indicate the hot spots. And these hot spots are located in an appropriate depth of the shallow area of the Earth's crust, which can be considered geothermal energy resources (e.g., Iceland-Nesjavellir Geothermal Power Plant). The rest of the areas on the tomography maps with various periods that has been shown with dark blue-green-yellow shades include colder and more rigid rocks and remnants of an old tectonic plate and is calm (aseismic), which represent cold spots. Cold spots usually cover a wide area and can cover tectonic plates and continents and may even include the mantle core, which is the source of cold (old) lava volcanic and some deep earthquakes.

Figure 8 illustrates the labeled major geological units (e.g., GC, EAAC, LC, BM); Volcanoes (e.g., El., Ar., Arg., Sab.); Basins (e.g., EBSB, SCB, RB, KB) to describe in this study. Figure 9 shows all the hot spots identified in this study for different periods.

Tomography velocity map at a period 5 s (Figure 9) shows 8 low-velocity hot spots (dark red shade). Hot spots 1, 4 and 5 in our study are located in the East Anatolian Accretionary Complex (EAAC) which is known for its thin lithosphere [*Şengör et al.*, 2003] in the east of Turkey. The depth of these hot spots is ~6 to 13.33 km (Figure 9).

Hot spot 1 is a small area near Kars mountain in NE Turkey known as the Erzurum-Kars Volcanic Plateau (EKVP). This part of the plateau has been formed by the eruptions during the Zanclean (~4.5 Ma) period, related to an earlier continental collision event between the Eurasian and Arabian continents ~15 Ma ago. The EKVP is composed mainly of andesitic and dacitic lavas and their trachytic equivalents intercalated with acidic ignimbrites and tuffs. In the northwest of Kars, an eroded stratovolcano is present which is possibly coeval with the plateau. It consists of a thick sequence of rhyolitic lavas, tuffs and perlitic-obsidian (e.g., [*Duru and Keskin*, 2020]).

Hot spots 2 and 3 are located in the central Armenian block (CAB) and north Armenia, respectively. Hot spot 2 is approximately located on the northern slope of Aragats volcano (depth of ~7 to 13.66 km), which may be the reason for the existence of magma (but at 10 s period this volcano is covered with a high-velocity anomaly (as a cold spot), which this feature might be explained by the old age of this volcano which does not express any activity for more than half million years). Based on some studies (e.g., [*Chernyshev et al.*, 2002; *Milyukov et al.*, 2017]) the Aragats center, one of the largest Quaternary volcanic centers in the Caucasus, is confined to the Aragats neovolcanic area located in the western part of Armenia, at the intersection of tectonic zones of a general Caucasian extension and the sublongitudinal Transcaucasus uplift. The development of the Pliocene-Quaternary volcanism of the Aragats area is defined by complex late collisional Geodynamics, which is related to global processes of the convergence of Eurasian and Arabian continental plates. Also, perhaps the emergence of a hot spot under the northern slope of the Aragats volcano in the tomography image of our study indicates new volcanic developments under this strato-volcano.

Hot spot 3 in our study covers a wide area such as Garni, Shoraghbyur, Yerevan, Avan salt dome, and Harazdan which were introduced from oil and gas resources (e.g., [*Jrbashyan et al.*, 2001]). The Paleocene and Lower Eocene of the subthrust section yielded oil-saturated cuttings and oil-cut mud and oil-stained cuttings were reported as features of the upper Eocene section in this area (thermo-

genic chemical interactions). By [*Milanovski*, 1962] about this hot spot, a detailed explanation is given as Sevan and Central Troughs. Due to the chemical interactions of in-Earth materials in oil-rich areas (which contain hydrocarbons) and gas resources, the temperature inside the Earth is high, and spots relevant to gas plumes are anomalously hot compared to the surrounding. The depth of this hot zone varies from 6.6 to 13.66 km. On the other hand, according to [*Jrbashyan et al.*, 2001], there are only a few oil and gas indications in the Sevan Trough. Gas shows and cuts of oil encountered during drilling on the southwestern shore of Lake Sevan (Yeranos-1) suggest that the molasse is prospective for hydrocarbons and country energy in the future.

As well as, in central Armenia, two Paleocene-Miocene flysch-molasse troughs, Central and Sevan, have been identified and several oil and gas shows have been reported from these troughs in Paleogene and Neogene strata. The Shoraghbyur High in the south-eastern part of the trough was the structural feature where shows were recorded from several intervals in the Shoraghbyur-1, where included an oil flow from a Paleocene horizon (3.474 to 3.589 m) and oil-cut mud from 3.640 to 3.634 m. The Paleocene and Lower Eocene of the subthrust section yielded oil-saturated cuttings. Oil-cut mud and oil-stained cuttings were reported as features of the upper Eocene section in Garni-1. Gas shows are reported in several wells over the Hrazdan structure. The Avan salt-dome area, between Hrazdan and the Vokchaberd Plateau, had oil shows in the Middle Miocene section (e.g., [*Klett*, 2016]). Therefore, the low-velocity anomaly in the Central Armenia Block in our study is located around these oil-gas areas (Yerevan, Sevan, Gavar, Martuni cities) and should be taken into consideration for the energy requirements of the country in the future.

As mentioned earlier, the hot spot 4 is situated in the EAAC, approximately beneath Ararat strato-volcanic structures (depth = ~6.6–13.66 km, velocity = 2 km/s) in the Julfa region, which could be due to the presence of a magma chamber beneath this volcanic complex. East-north foothills of this volcanic complex are affected by sediments of the Aras river, which is limited by the uplifted basement of the Ararat volcanos to the south and by the Hrazdan Transverse Fault Zone to the west.

Also, some seismic tomography study indicates a magma reservoir at great depths (20–30 km) below the Ararat volcano [*Özgür Karaoğlu et al.*, 2017]. Geochemical constraints on some of the later-formed rocks suggest an interaction between a shallow chamber (8–10 km) and the deep reservoir of approximately 0.5 Ma. This depth is consistent with the result of our study in a period of

5 s (depth 7–13 km; Figure 8). Although, slow velocities under regions of active volcanism do not require hot spot magmatism.

Low-velocity (dark red area) that we assume as the hot spot 5, is approximately located in the northeast of Lake Van and includes Tendurek, Suphan and Nemrut mountains. A study of [*Oyan*, 2018] shows collision related to Quaternary Mafic Volcanism to the north of Lake Van that has occurred by eruptions from both volcanic centers and extensional fissures trending approximately north-south. Low-velocity anomaly and the existence of the hot springs around these mountains signify high-temperature rocks. Also, the volcanic products in this area consist of mildly alkaline lavas and calculations based on crustal temperatures and Curie point depths indicate that the magma chamber might have been located at a depth of around 6–8 km, within the upper crust.

For the period of 5 s in our study, this property has been shown at a depth of 6 to 13.66 km. We infer, that perhaps, the molten material beneath the Ararat volcano complex and the mountains around Lake Van are quite interconnected. As well as, the pattern of concepts of hot spots 1, 4, and 5 is almost the same, as these spots are situated in the EAAC which is known for its thin and hot (shallow) lithosphere structure [*Angus et al.*, 2006]. So, there is a possibility of the hot rocks and the high temperature inside the Earth of this region as a hot spot.

The hot spots 6 and 7 are located in NW Iran near the north part of Sahand volcano and the southeastern segment of the north Tabriz fault. This fault is responsible for destructive earthquakes in Tabriz (e.g., M= 7.7, 1721). The epicenter of this earthquake is located right in the hot zone of 6. It is clear that these hot spots are perhaps due to the interactions of the rocks of this famous active fault or magma chamber beneath the Sahand volcano. A study has reported evidence of limited volcanic eruptions in the South of the Tabriz fault (Sahand block) that are characterized by ages ranging from 11 Ma to the present (era 4). The 11 Ma lavas have an alkaline potassic to ultrapotassic composition [*Aghazadeh et al.*, 2010]. Also, the existence of the low-velocity zones beneath the NW Iran volcanoes in our results at a period of 5 s could be due to the high temperature of the volcanic rocks or shallow magma chamber beneath this region. The existence of the hot springs around these volcanoes signifies these high-temperature rocks. In contrast, beneath the Sahand volcano, a high-velocity zone is observed that could be due to the low-temperature volcanic rocks or a deeper magma chamber at a depth of ~30.8 km.
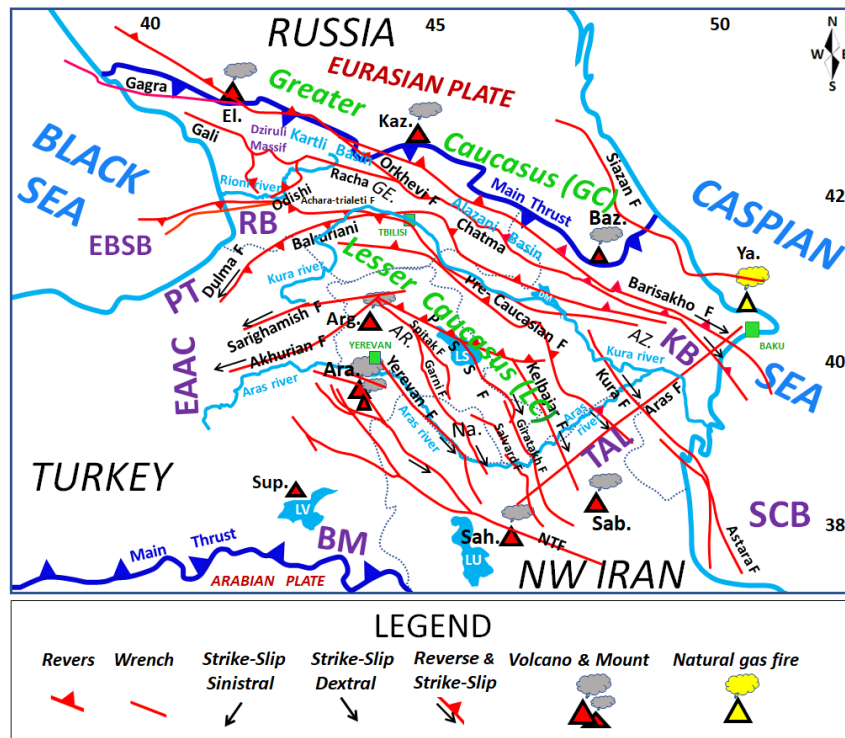
Figure 7: Geological units, faults, volcanoes, rivers, and basins that were used for the interpretation of the 2D tomography maps in the study area. Abbreviations: F= Fault, Sab.= Sabalan, Sah.= Sahand, Sup.= Suphan, Ara.= Ararat, PT= Pontide, BM= Bitlis Massif, EAAC= East Anatolian Accretionary Complex, Arg.= Aragats, El.= Elbrus, Kaz.= Kazbek, Baz.= Bazarduzu, Ya.= Yanardag (natural gas fire on a hillside), Na.= Nakhchivan, GO.= Georgia, AR.= Armenia, AZ= Azerbaijan, LV= Lake Van, LU= Lake Urmia, LS= Lake Sevan, MD= Mingachevir Dam, TAL= Talesh, KB= Kura Basin, RB = Rioni Basin, SCB= South Caspian Basin, EBSB= Eastern Blake Sea Basin, PSSF= Pambak-Sevan-Syunik Fault, and NTF= North Tabriz Fault. The seismic sources (faults) of the Caucasus are retrieved from [*Adamia et al.*, 2011].

Hot spot 8 is located near a segment of the Salvard fault in the northeast of Nakhichevan (Figure 9). According to several studies (e.g., [*Danelian et al.*, 2014; *Sokolov*, 1977]), exposures of Jurassic sequences are located in Nakhichevan and in Iran, where a 500 m -thick Lower and Middle Jurassic sedimentary sequence overlies Upper Triassic strata. Lower Cretaceous deposits are absent on the south Armenian block and the Triassic-Jurassic deposits are unconformably overlain by Cenomanian reefal limestones that are covered by marls. Upper Devonian (the fourth period of the Paleozoic era) and Permian (the fifth period of the Paleozoic era) rocks could be petroleum source rocks [*Sosson et al.*, 2010]. Silurian and Lower and Middle Devonian marine clastic and carbonate rocks crop out in Nakhichevan and are presumed to be present in Armenia. Our study has shown this property in a period of 5 s at a depth of 6 to 9.5 km (hot spot 8). The presence of petroleum and carbonate rocks resources and chemical-thermal activity related to it can be a sufficient reason for the hot temperature inside the Earth in this area as a hot spot.

The tomography velocity map of the 10 s period shows the hot spots 9, 10, 11 and 12, which are located in the Greater Caucasus. These hot spots are including the eastern Black Sea basin (EBSB) and a segment of the Odishi fault in the Rioni basin (9); the Terek basin in Russia and NSW of Kazbek neovolcanic center (10); the Chatma region in the east of Georgia (11), and South Caspian Basin (12). These hot spots follow the same pattern as described for hot spots 1 to 8.

As mentioned, the low-velocity anomaly beneath the volcanoes in the depth associated with this period (14 to 28.66 km), reveals the presence of magma and the magmatic reservoir and sediments. Although, slow velocities under regions of active volcanism complexes do not require hot Spot magmatism. Broad low-velocity zones are observed in the SCB-Kura basins, and the Baku region (hot spot 12), which according to a study by [*Bochud*, 2011], the presence of abundant major oil and gas fields (hydrocarbons) in the Baku-Kura region could be the reason for the low surface wave velocity in this area. Sediments reach 5–7 km and more in part of the Rioni-Kura foredeep
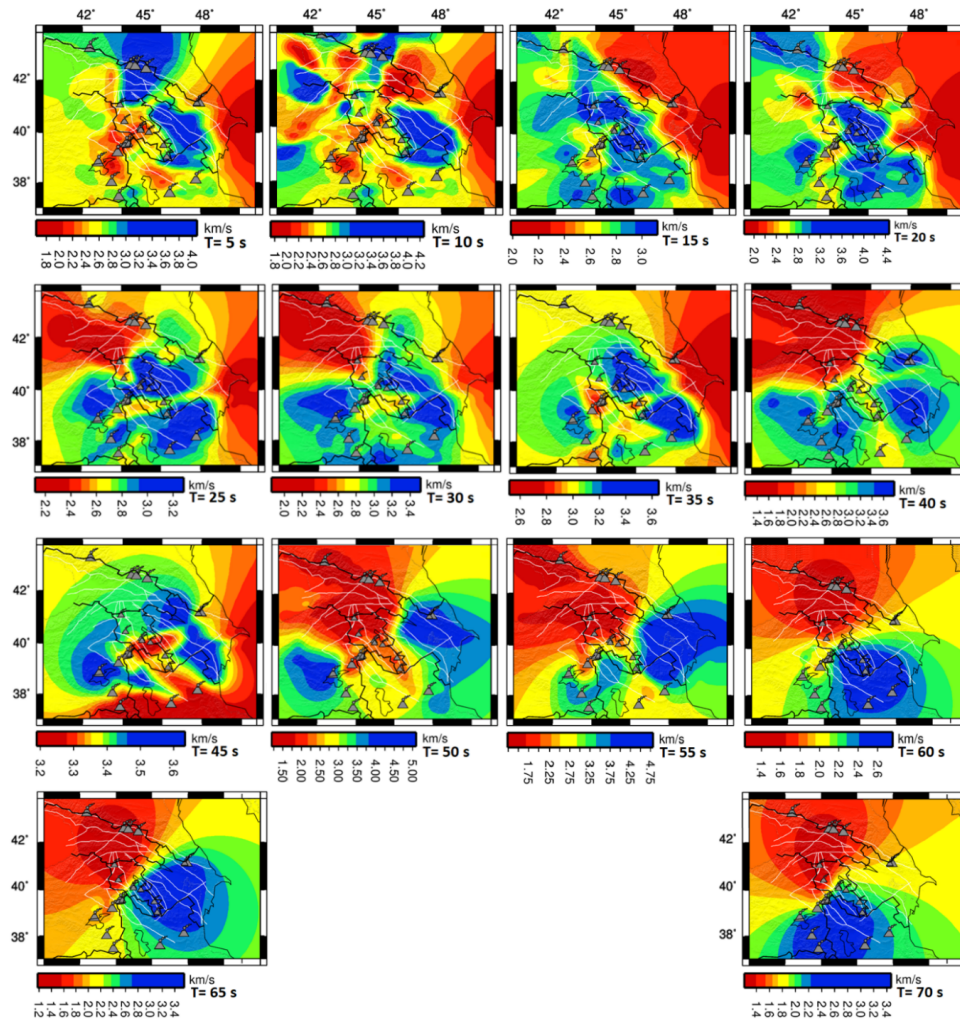
Figure 8: Rayleigh wave group velocity tomography maps for short-periods (5, 10, 15, 20, 25 s); medium-periods (30, 35, 40, 45, 50 s), and long-periods (55, 60, 65, 70 s) used in this study. The white lines are faults and the gray triangles are volcanoes and mounts.

basin [*Jrbashyan et al.*, 2001]. The Black Sea is generally thought to have a basement of oceanic crust that is overlain with 10–20 km of sediment. Similarly, the basement of the Southern Caspian Sea basin has geophysical attributes like that of thick oceanic crust and is overlain by ~20 km of sedimentary cover [*Mangino and Priestley*, 1998]. The presence of abundant major oil and gas fields (hydrocarbons) in the Baku-Kura-Terek region could be another reason for the low surface wave velocity [*Bochud*, 2011].

Dark red low-velocity area which we assume to be the hot spot 13, includes the Elbrus volcanic complexes, Dzirula Massif, Kazbek neovolcanic center, and Yanardag (natural gas fire on a hillside) in the Greater Caucasus. The low velocity anomaly beneath the volcanoes in the depth associated with ~30.8 km and 158.6 km in these periods reveals the presence of magma and the magmatic reservoirs and mantle plume. In our tomography map with long-period of 70 s (equiv-

alent to a depth of 158.6 km); Azerbaijan, Kura-South Caspian basins, and Talesh heights are covered with high-velocity, which we suggest cold lithosphere roots for deep areas. On the contrary, the low-velocity in the Greater Caucasus, eastern Black Sea basin, and EAAC are resulting in a very thin (shallow) lithosphere and hot asthenosphere (in great depth). The hot spots in a period of 15 s follow the pattern described in periods of 5 and 10 s.

The results at a period of 40 s (depth ~100 km) show a low-group velocity for most parts of NW Iran, Talesh heights, South Caspian Basin (SCB), and the Astara region, which could be due to the warm upper mantle in these regions. We determined the hot spot 14 in NW Iran, where, according to some studies (e.g., [*Sugden et al.*, 2018]), the mid-lithosphere magma source has a distinct composition compared to the base of the lithosphere, that is argued to be the result of the increased retention of metasomatic components in
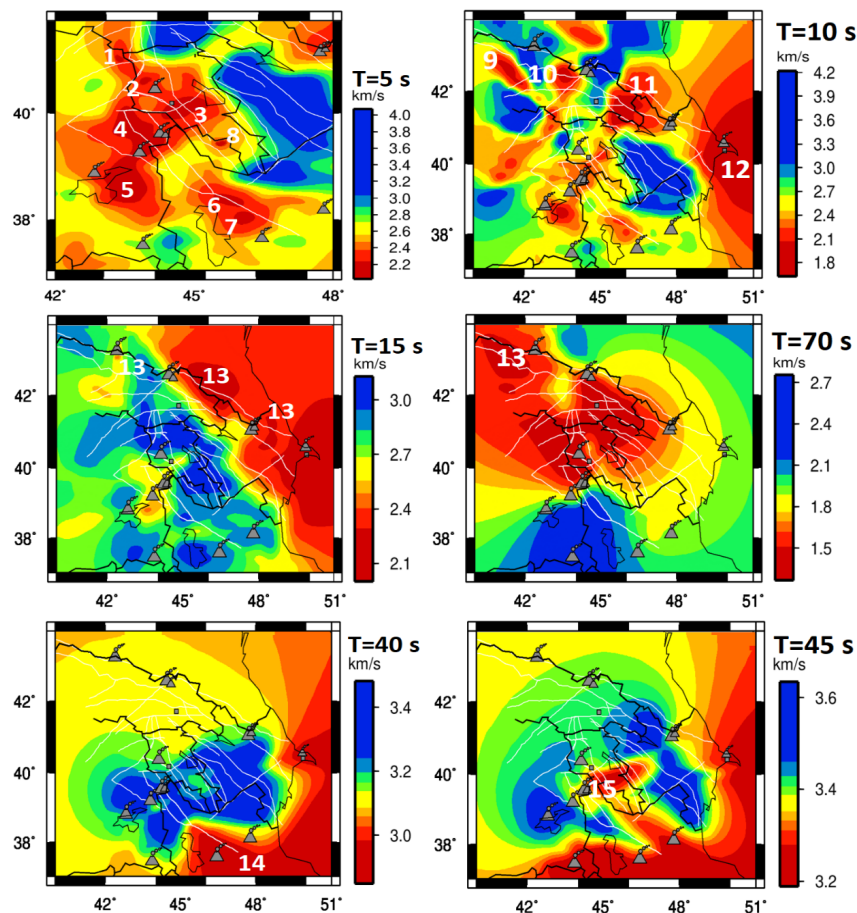
Figure 9: Labeled areas 1 to 15 are the major low-velocity with dark red shade (slow) that we assumed as hot spots and the rest of the areas with dark blue-green-yellow shades are high-velocity (fast) or cold spots, which represent the remnants of an old tectonic plate that has sunk beneath the Earth's plates in our study. Greater Caucasus hot spots are shown with the 13. The white lines are faults and the gray triangles are volcanoes and mounts.

phases such as apatite and amphibole, that are stabilized by lower temperatures prior to magma generation. Also, partial melts of the deep lithosphere ~120 km (in our study 111 km) and mid-lithosphere sources to give a composition intermediate between magmas from the northern Lesser Caucasus and NW Iran could be the reason for this extensive hot spot, in addition, leads our mind to onset the low-velocity zone (LVZ, depth of ~104, Figure A.2) discontinuity.

A wide very low-velocity anomaly at a period of 45 s is observed in Sahand, Sabalan, Bitlis, Nakhchivan, Astara, South Caspian Basin, lake Urmia, and especially in the South Armenia Block (SAB). We infer that the hot spot 15 is situated in the South Armenia Block (SAB). About the low-velocity in Nakhchivan, Syunik-Gegham-Vardenis highlands, or SAB, we interpret that due to the upper Devonian (the fourth period of the Paleozoic era) and Permian (the fifth period of the Paleozoic era) rocks. They could be petroleum source rocks. Silurian and Lower and Middle Devonian

marine clastic and carbonate rocks crop out in Nakhichevan and are presumed to be present in Armenia (e.g., [*Sosson et al.*, 2010]) (also, see the explanation of hot spot 8).

The Gegham volcanic group in Armenia also matches the location of the low-velocity anomaly. Besides this, in a study of [*Sugden et al.*, 2018], a diagram of depth vs. temperature of melting shows that after the depth of ~80 (1100 °C) and 150 km (1400 °C), the temperature has a significant increase in Gegham, Syunik, and Vardenis. So, we propose that the interactions and intrusion of very hot molten material from the upper mantle into the asthenosphere-lithosphere discontinuities for creating hot spot 15 are not unexpected.

The rest of the areas with dark blue-green-yellow shades are cold spots, which represent the remnant of an old tectonic plate that has sunk beneath the Earth's plates.

The results for the long-periods are different, and in this case (deep areas with depth ~180 km), the Rayleigh waves are more influenced by the ve-

locity structure of the uppermost mantle. We argue at these periods the low-velocity anomalies are mainly due to the absence (thinning) of a lithospheric mantle or a thin mantle lid, while high velocities can be related to the presence of a stable continental mantle lid or of an oceanic-like lithosphere. Our interpretation is in good agreement with some studies (e.g., [*Zabelina et al.*, 2016] and [*Koulakov et al.*, 2012]).

Seismic waves pass through the lithosphere-asthenosphere very slowly and wave velocity reduction from lithosphere to asthenosphere, could be caused by the presence of a very small percentage of melt in the asthenosphere. The upper mantle low-velocity zone (LVZ) is a depth interval with slightly reduced seismic velocity compared to the surrounding depth intervals. The zone is present below a relatively constant depth of 100 km (in our study depth of 104 km, Figure A.2) in most continental parts of the world [*Thybo*, 2006]. And the LVZ extends from about 65 to 220 km depth in the ocean basins [*Presnall and Gudfinnsson*, 2011].

Therefore, the hot wide area is not unexpected. Figure A.2 has depicted the approximate depth of Moho, LAB, and LVZ for this study. In the Lesser Caucasus, there is a link between volcanic manifestations and low-velocity patterns, but it is not as clear as in the Great Caucasus.

At long-period (55–70 s and approximate depth = 200 km), velocity structures of our tomographic maps indicate ultrahigh-velocity anomalies (5.04 km/s) and ultralow-velocity (1.4 km/s) zones (Figure 8). We infer the deep ultrahigh-velocity anomalies may be the broken off cold lithosphere generated slabs were sinking into the mantle transition zone and very-hot upper mantle with low mantle lid (cap). In contrast, for ultralow-velocity regions, it is thought that the upper mantle has been rejuvenated by a phase of the upwelling hot mantle, and this metasomatic refertilization of the upper Cratonic mantle has increased its density and reduces seismic velocity and rocks experience temperatures above 1300–1600 °C at these depths.

Also, according to the depth-temperature diagram (e.g., [*Sugden et al.*, 2018]), at these depths, some interactions such as the onset of dry melting in the convecting mantle cause an increase in temperature and density conflicts tension. So, we propose that at the depths joint between the lithosphere-asthenosphere-upper mantle anomalies accumulation, inhomogeneities, and antagonistic behaviors are prevalent in surface wave velocity variations. In these regions, due to continuous temperature changes caused by the plate tectonic activity, the effect of active liquids penetrated by the asthenosphere, subsidence, uplifts, hot asthenospheric diapirs intrusion, the velocity

of waves experiences many fluctuations (e.g., [*Sugden et al.*, 2018]).

Also, as mentioned, seismic waves traverse slowly from the lithosphere-asthenosphere boundary (LAB), which is known as the low-velocity zone (LVZ), and then enter the upper mantle (Figure A.2). Poor coverage of ray paths in this part of the study area (T= 60, 65, and 70 s) leads to stretching and smearing (butterfly-shaped areas) by this feature toward the northwest and southeast of the study area. In these periods, due to some reasons such as plate tectonic activities, hot asthenospheric diapirs intrusion, the effect of active liquids penetrated by the asthenosphere, subsidence, uplifts, and mantle plumes the temperature changes constantly, and therefore, the surface waves have variable behavior.

6 DISCUSSION

Hot spots and related structures in the mantle are very important to understand the dynamics of the Earth and the modes of heat transfer inside the planet and there are evidences for subduction or underplating crust in these regions. Here, we're looking for cold and hot spots inside the Earth. Therefore, using the 2D tomography technique and increasing-decreasing the wave velocity anomalies in different geological units of the study area, hot and cold spots were determined.

In other words, using the commentary seismic tomography images results from within the Earth, we are looking for the following results in the period of 5 to 70 seconds: 1. Dark blue-green-yellow shades mean colder and stiffer rock (Cold Spots – areas with fast wave velocity), which are the remnants of an old tectonic plate that has been subducted underneath the Earth's plates (large cold and aseismic area during million years). 2. Dark red-orange shades mean warmer and weaker regions (hot spots- areas with slow wave velocity).

So, our tomography maps show the hot zones with dark red shade, where, there is diapirs intrusion, mantle plumes, a chain of volcanoes, and fault activity. And the maps with dark blue-green-yellow shades show the cold zones, where, oceanic plates have sunk into the Earth's interior in the past, supporting the idea that dense slabs of the oceanic crust may penetrate to the lower mantle (underlie areas).

In the study area, the highest number of hot and cold spots are corresponding to the short periods (T= 5 to 20 s) and approximately 13 major hot spots (6.6 < depth < 30.8 km; 1.4 < velocity < 2 km/s) for different geological units of the Caucasus were identified. The location of these hot and cold spots is in good agreement with the results of mentioned tomographic studies in this region.

Since the geothermal resources are shallow-crustal phenomena (a few km above the crust), these short-period hot spots, are located in an appropriate depth of the shallow area of the Earth's crust as geothermal energy for humans. In fact, this is the first study to determine and interpret the hot-cold spots of the Caucasus region using Rayleigh surface wave velocity, and so far, no study has been conducted that directly examines the *hot-cold spots in the Caucasus* by using decreasing and increasing the surface wave velocity.

As well, identified hot spots and cold spots (15 regions) follow physical processes within the Earth and magma generation in Figure A.1 steps. Based on tomographic maps in periods of 5 to 70 s and geological evidences, 15 hot spots with dark red shades in the study area were determined and analyzed and the rest of the areas with dark blue-green-yellow shades are cold spots, which represent the remnants of an old tectonic plate that has sunk beneath the Earth's plates.

As an overall result for three groups of short, medium, and long periods in the Caucasus, tomography maps with distinct velocities for the short periods (T= 5–25 s; equivalent depth of 6.6–53.33 km) are more sensitive to the structure of the upper-middle crust. Based on the reduction and increase in the surface wave velocity, these periods represent sediments in the basins, hydrocarbon resources, molten material, and magma chambers beneath volcanoes and Moho discontinuity which these areas can be considered *temporary and unstable* hot and cold spots inside the Earth.

Of course, as mentioned, slow velocities under regions of active volcanism complexes do not require hot spot (i.e., plume-related) magmatism. These could simply reflect decompression melting or crustal melting following slab-rollback, delamination, or breakoff.

In tomographic maps with medium-periods (T= 30–45 s; equivalent depth of 68 to 108 km) the Azerbaijan, Kura-South Caspian basins, and Talesh heights are covered with high-velocity, which according to the results of the previous studies this condition is due to the cold lithosphere roots. On the contrary, due to the presence of a very thin lithosphere and hot asthenosphere, the low-velocity anomaly in the Eastern Greater Caucasus, Eastern Black Sea Basin, Eastern Anatolia, and NW Iran are observed. These can be considered *temporary and semi-stable* hot and cold spots inside the Earth.

In long-period tomographic maps ($50 \leq T \leq 70$ s; depth of ~180 km), there are ultrahigh-velocity anomalies (dark blue) under the South Caspian Sea-Kura Basins, Baku, and even are spread to the Talesh heights, NW Iran, and the Bitlis Massif, while, a wide area is covered with ultralow-velocity (dark red). These deep ultrahigh-velocity anomalies may be due to the broken-off cold lithosphere-generated slabs that were sinking into the mantle transition zone and very-hot upper mantle with a thin mantle lid (cap). Whereas the subduction system (e.g., Eastern Greater Caucasus and South Caspian Sea basin) and asthenosphere with significant amounts of melt (e.g., Armenia, Georgia, EAAC, and Western Greater Caucasus) is the major factor in creating the ultralow-velocity zone, which these areas can be considered *permanent and stable* hot and cold spots inside the Earth.

7 CONCLUSIONS

In this study, we have performed 2D tomography maps of Rayleigh wave for the entire Caucasus using the method developed by Yanovskaya-Ditmar. The derived 2D tomography velocity anomaly maps of Rayleigh wave dispersion curves were carefully verified using the fundamental mode of vertical component (Z) of earthquake waveform energy to identify hot-cold spots, better understand the regional tectonic activities, faults activities, and lithospheric blocks interactions as geothermal resources and surface waves velocity variations in the ongoing collision-compressed edge zone of the Eurasian-Arabic plates. These maps show excellent agreement with many of the geological features of the Caucasus territory, such as the Volcanoes Complex, Troughs, Uplifts, and Basins.

Also, 15 low-velocity areas (hot spots) were identified. These are the hot spots 10, 11, and 13 (in Greater Caucasus); 1, 4, and 5 (EAAC); 2, 3, and 15 (Lesser Caucasus-Armenia); 6, 7 and 14 (NW Iran); 12 in the South Caspian Sea Basin; 9 (Rioni-Eastern Black Sea Basin) and 8 are located NW of Nakhchivan and are in good agreement with previous studies and geological evidences. The rest of the areas with dark blue-green-yellow shades are cold spots, which represent the remnants of an old tectonic plate that has sunk beneath the Earth's plates. The hot spots close to the Earth's surface during short periods can be considered geothermal resources to provide the heat energy for cities and power plants (e.g., hydrothermal of Sabalan volcano in Iran-Ardabil and Iceland-Nesjavellir Geothermal Power Plant).

Network of Turkey (DDA), National Seismic Network of Azerbaijan and National Seismic Network of Georgia who provided some of the seismic data used in this study. Many of the figures in this paper were prepared using GMT (Wessel & Smith 1995), and the authors thank them. We also thank the Institute of Geophysics of the University of Tehran, which managed and supported this study in the framework of the educational mission (2016–2018). Special thanks to Michael Smith (USA) & Natasha Lewis (USA) for editing the grammar of the article.

References

Adamia, S., G. Zakariadze, T. Chkhotua, N. Sadradze, N. Tsereteli, A. Chabukiani, and A. Gventsadze, Geology of the Caucasus: A Review, *Turkish Journal of Earth Sciences*, doi:10.3906/yer-1005-11, 2011.

Aghazadeh, M., A. Castro, N. R. Omran, M. H. Emami, H. Moinvaziri, and Z. Badrzadeh, The gabbro (shoshonitic)–monzonite–granodiorite association of Khankandi pluton, Alborz Mountains, NW Iran, *Journal of Asian Earth Sciences*, *38*(5), 199–219, doi:10.1016/j.jseaes.2010.01.002, 2010.

Angus, D. A., D. C. Wilson, E. Sandvol, and J. F. Ni, Lithospheric structure of the Arabian and Eurasian collision zone in eastern Turkey from S-wave receiver functions, *Geophysical Journal International*, *166*(3), 1335–1346, doi:10.1111/j.1365-246x.2006.03070.x, 2006.

Backus, G., and F. Gilbert, The Resolving Power of Gross Earth Data, *Geophysical Journal International*, *16*(2), 169–205, doi:10.1111/j.1365-246x.1968.tb00216.x, 1968.

Bavali, K., K. Motaghi, F. Sobouti, A. Ghods, M. Abbasi, K. Priestley, G. Mortezanejad, and M. Rezaeian, Lithospheric structure beneath NW Iran using regional and teleseismic travel-time tomography, *Physics of the Earth and Planetary Interiors*, *253*, 97–107, doi:10.1016/j.pepi.2016.02.006, 2016.

Bochud, M., Tectonics of the eastern greater caucasus in Azerbaijan, Phd thesis in tectonics and general geology, University of Fribourg, Switzerland, geoFocus, 30, thesis No: 1733, 2011.

Chernyshev, I. V., V. Lebedev, S. N. Bubnov, M. M. Arakelyants, and Y. V. Gol'tsman, Isotopic geochronology of Quaternary volcanic eruptions in the Greater Caucasus, *Geochemistry International*, *40*, 1042-1055, 2002.

Copley, A., and J. Jackson, Active tectonics of the Turkish-Iranian Plateau, *Tectonics*, *25*(6), doi:10.1029/2005tc001906, 2006.

Danelian, T., A. Zambetakis-Lekkas, G. Galoyan, M. Sosson, G. Asatryan, B. Hubert, and A. Grigoryan, Reconstructing Upper Cretaceous (Cenomanian) paleoenvironments in Armenia based on Radiolaria and benthic Foraminifera; implications for the geodynamic evolution of the Tethyan realm in the Lesser Caucasus, *Palaeogeography, Palaeoclimatology, Palaeoecology*, *413*, 123–132, doi:10.1016/j.palaeo.2014.03.011, 2014.

Ditmar, P. G., and T. B. Yanovskaya, Generalization of Backus-Gilbert method for estimation of lateral variations of surface wave velocities, *Izvestia*, *Phys. Solid Earth*, *23*(6), 470–477, 1987.

Duru, O., and M. Keskin, Magmatic Evolution of the ALADAĞ Volcanic System and Southern Edge of the Erzurum-Kars Volcanic Plateau (SARIKAMIŞ, City of Kars, NE Turkey), doi:10.5194/egusphere-egu2020-21626, 2020.

Foulger, G. R., *Plates vs Plumes: A Geological Controversy*, Wiley-Blackwell, 2010.

Gheitanchi, M. R., Crustal structure in NW in Iran, revealed from the 1990 Rudbar aftershock sequence, *J. Earth Space Phys.*, (23), 7–14, 1996.

Golonka, J., Plate tectonic evolution of the southern margin of Eurasia in the Mesozoic and Cenozoic, *Tectonophysics*, *381*(1-4), 235–273, doi:10.1016/j.tecto.2002.06.004, 2004.

Hatzfeld, D., and P. Molnar, Comparisons of the kinematics and deep structures of the Zagros and Himalaya and of the Iranian and Tibetan plateaus and geodynamic implications, *Reviews of Geophysics*, *48*(2), doi:10.1029/2009rg000304, 2010.

Herrmann, R. B., Computer Programs in Seismology: An Evolving Tool for Instruction and Research, *Seismological Research Letters*, *84*(6), 1081–1088, doi:10.1785/0220110096, 2013.

Ismail-Zadeh, A., S. Adamia, A. Chabukiani, T. Chelidze, S. Cloetingh, M. Floyd, A. Gorshkov, A. Gvishiani, T. Ismail-Zadeh, M. K. Kaban, F. Kadirov, J. Karapetyan, T. Kangarli, J. Kiria, I. Koulakov, J. Mosar, T. Mumladze, B. Müller, N. Sadradze, R. Safarov, F. Schilling, and A. Soloviev, Geodynamics, seismicity, and seismic hazards of the Caucasus, *Earth-Science Reviews*, *207*, 103222, doi:10.1016/j.earscirev.2020.103222, 2020.

Jackson, J., Partitioning of strike-slip and convergent motion between Eurasia and Arabia in eastern Turkey and the Caucasus, *Journal of Geophysical Research*, *97*(B9), 12471, doi:10.1029/92jb00944, 1992.

Jrbashyan, R., G. Chlingaryan, Y. Kagramanov, A. Karapetyan, M. Satian, Y. Sayadyan, and H. Mkrtchyan, Geology of Meso-Cenozoic Basins in Central Armenia, with Comment on Indications of Hydrocarbons, *Search and Discovery*, (30007), 2001.

Karapetyan, J. K., R. S. Sargsyan, K. S. Kazaryan, B. V. Dzeranov, B. A. Dzeboev, and R. Karapetyan, Current state of exploration and actual problems of tectonics, seismology and seismotectonics of Armenia, *Russian Journal of Earth Sciences*, *20*(2), 1–14, doi:10.2205/2020es000709, 2020.

Klett, T. R., Geology and assessment of the undiscovered, technically recoverable petroleum resources of Armenia, 2013, doi:10.3133/ds69pp, 2016.

Koulakov, I., I. Zabelina, I. Amanatashvili, and V. Meskhia, Nature of orogenesis and volcanism in the Caucasus region based on results of regional tomography, *Solid Earth*, *3*(2), 327–337, doi:10.5194/se-3-327-2012, 2012.

Mangino, S., and K. Priestley, The crustal structure of the southern Caspian region, *Geophysical Journal International*, *133*(3), 630–648, doi:10.1046/j.1365-246x.1998.00520.x, 1998.

Martin, R., M. Krasovec, S. Romer, T. O'Connor, E. G. Bombolakis, Y. Sun, and N. Toksoz, Caucasus Seismic Information Network: Data and Analysis Final Report, *Tech. rep.*, doi:10.2172/899760, 2007.

Milanovski, E. E., Sevan Basin, Geology of Armenian SSR, *Geomorphology*, (1), 133–135, (In Russian), 1962.

Milyukov, V., E. Rogozhin, A. Gorbatikov, A. Mironov, A. Myasnikov, and M. Stepanova, Contemporary State of the Elbrus Volcanic Center (The Northern Caucasus), *Pure and Applied Geophysics*, *175*(5), 1889–1907, doi:10.1007/s00024-017-1595-x, 2017.

Oyan, V., Geochemical and petrologic evolution of Otlakbaşı basaltic volcanism to the east of Lake Van, *Bulletin Of The Mineral Research and Exploration*, pp. 10–20, doi:10.19111/bulletinofmre.427782, 2018.

Özgür Karaoğlu, A. Elshaafi, M. K. Salah, J. Browning, and A. Gudmundsson, Large-volume lava flows fed by a deep magmatic reservoir at Ağrı Dağı (Ararat) volcano, Eastern Turkey, *Bulletin of Volcanology*, *79*(2), doi:10.1007/s00445-016-1098-0, 2017.

Perkins, S., Seismic tomography uses earthquake waves to probe the inner Earth, *Proceedings of the National Academy of Sciences*, *116*(33), 16159–16161, doi:10.1073/pnas.1909777116, 2019.

Presnall, D. C., and G. H. Gudfinnsson, Oceanic Volcanism from the Low-velocity Zone – without Mantle Plumes, *Journal of Petrology*, *52*(7-8), 1533–1546, doi:10.1093/petrology/egq093, 2011.

Şengör, A. M. C., S. Özeren, T. Genç, and E. Zor, East Anatolian high plateau as a mantle-supported, north-south shortened domal structure, *Geophysical Research Letters*, *30*(24), doi:10.1029/2003gl017858, 2003.

Skobeltsyn, G., R. Mellors, R. Gök, N. Türkelli, G. Yetirmishli, and E. Sandvol, Upper mantle S wave velocity structure of the East Anatolian-Caucasus region, *Tectonics*, *33*(3), 207–221, doi:10.1002/2013tc003334, 2014.

Sokolov, S. D., *Olistostrome Series and Ophiolite Nappes of the Lesser Caucasus*, Nauka, Moscow, (In Russian), 1977.

Sosson, M., N. Kaymakci, R. Stephenson, F. Bergerat, and V. Starostenko, Sedimentary basin tectonics from the Black Sea and Caucasus to the Arabian Platform: introduction, *Geological Society, London, Special Publications*, *340*(1), 1–10, doi:10.1144/sp340.1, 2010.

Sugden, P. J., I. P. Savov, M. Wilson, K. Meliksetian, G. Navasardyan, and R. Halama, The Thickness of the Mantle Lithosphere and Collision-Related Volcanism in the Lesser Caucasus, *Journal of Petrology*, *60*(2), 199–230, doi:10.1093/petrology/egy111, 2018.

Thybo, H., The heterogeneous upper mantle low velocity zone, *Tectonophysics*, *416*(1-4), 53–79, doi:10.1016/j.tecto.2005.11.021, 2006.

Wilson, J. T., A Possible Origin Of The Hawaiian Islands, *Canadian Journal of Physics*, *41*(6), 863–870, doi:10.1139/p63-094, 1963.

Wright, L., Earth's interior: Raising hot spots, http://www.geotimes.org/nov00/hotspot.html, geotimes, American Geological Institute, 2000.

Yanovskaya, T. B., Resolution estimation in the problems of seismic ray tomography, *Izv. Phys. Solid Earth*, (33), 762–765, 1997.

Yanovskaya, T. B., and P. G. Ditmar, Smoothness criteria in surface wave tomography, *Geophysical Journal International*, *102*(1), 63–72, doi:10.1111/j.1365-246x.1990.tb00530.x, 1990.

Yanovskaya, T. B., E. S. Kizima, and L. M. Antonova, Structure of the crust in the Black Sea and adjoining regions from surface wave data, *Journal of Seismology*, (2), 303–316, 1998.

Zabelina, I., I. Koulakov, I. Amanatashvili, S. E. Khrepy, and N. Al-Arifi, Seismic structure of the crust and uppermost mantle beneath Caucasus based on regional earthquake tomography, *Journal of Asian Earth Sciences*, *119*, 87–99, doi:10.1016/j.jseaes.2016.01.010, 2016.

A Appendix
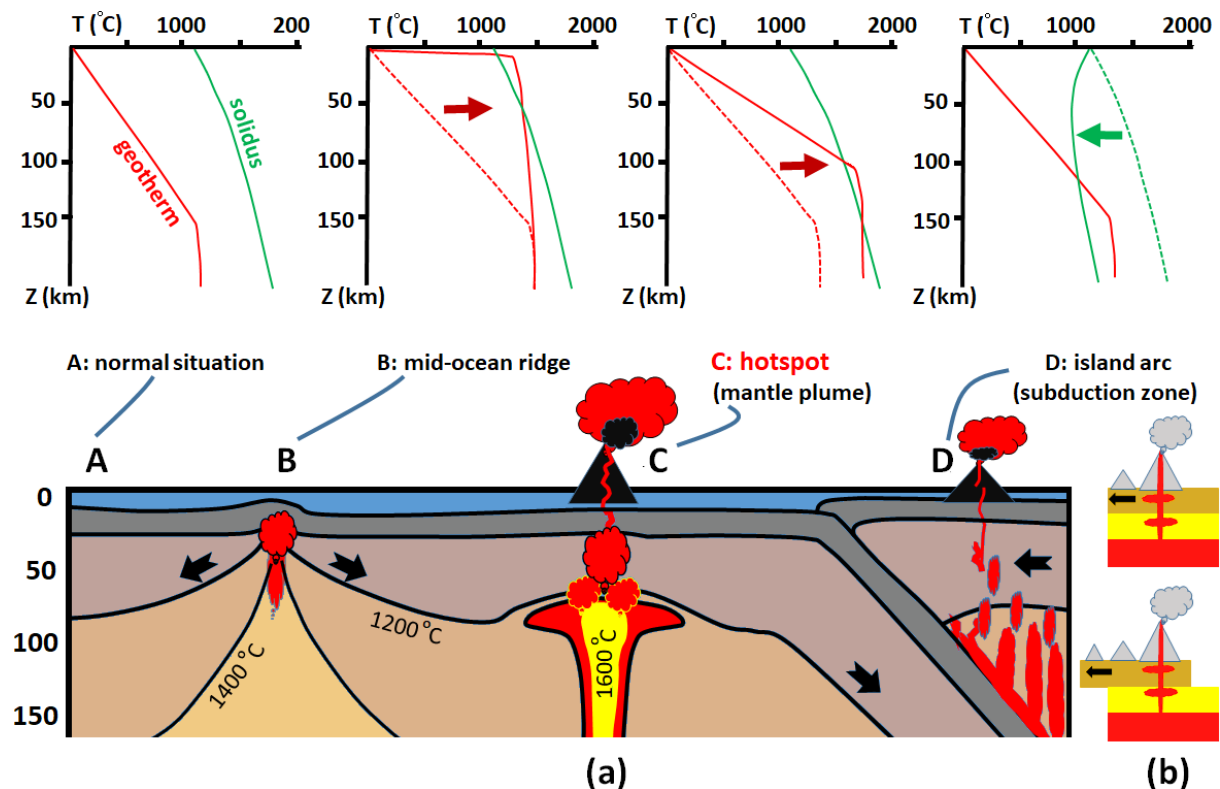
Figure A.1: (a) Schematic diagram showing the physical processes inside the Earth that lead to the generation of magma that partial melting begins above the fusion point b) Shows a cross-section through the Earth's lithosphere (yellow) with magma rising from the mantle (red). Figure retrieved from [https://geo.libretexts.org/Courses/Lumen_Learning/Book%3A_Geology_(Lumen)/11%3A_Module_9-_Volcanoes/11.09%3A_Reading-_Volcanoes_Hotspots]. The graphs show the geothermal curves (the temperature curve inside the Earth, red) and the solidus (the temperature where rock starts to melt, green). When the two curves cross each other, magma is generated by partial melting. A) The curves do not cross- no magma is generated B) at mid-ocean ridges magma generation occurs at quite shallow depths due to high temperatures and very thin lithosphere C) over mantle plumes magma generation occurs at larger depths due to even higher temperatures, but thicker lithosphere D) over subducting slabs magma generation occurs at larger depths due to lowering of melting temperature of the rock by fluids released from the slab.
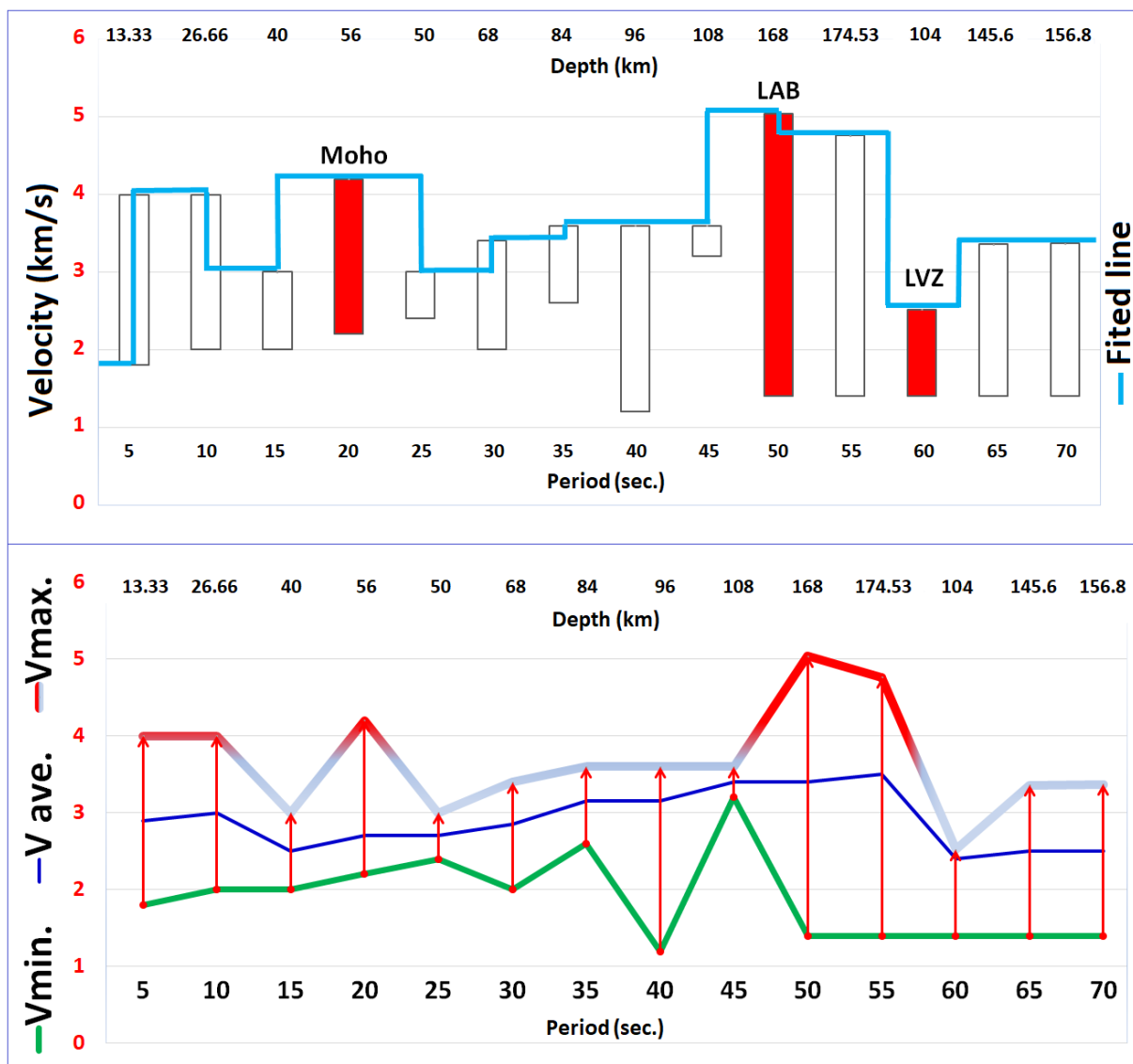
Figure A.2: Velocity variations versus depth in different periods and approximate location of Moho, Lithosphere-Asthenosphere Boundary (LAB), and Low-Velocity Zone (LVZ) with respect to the group velocity in this study.